



Optimization of Cabin Mounting System for Tractor using a Genetic Algorithm

Min-Woo Kang¹ · Hyun-Woo Han¹ · Young-Jun Park^{1,2,3}

Received: 17 January 2024 / Revised: 7 February 2024 / Accepted: 13 February 2024 / Published online: 26 February 2024
© The Author(s) 2024, corrected publication 2024

Abstract

Purpose To analyze the behavior of a tractor cabin mounting system, a six-degrees-of-freedom (6-DOF) simulation model was developed, and a genetic algorithm was integrated into the model to optimize the design variables of the cabin mounting system. The performance and characteristics of the optimized cabin-mounting system were analyzed.

Methods Eigenvalue analysis was performed using the developed model. Rigid-body mode decoupling theory was applied to optimize the design variables, and the energy decoupling method (EDM) was used to evaluate the degree of rigid-body mode decoupling. The design variables were optimized using NSGA-II genetic algorithm. Optimizations for two cases (Case #1: optimizing the stiffness and position of the mounts; Case#2: optimizing only the stiffness of the mounts) were conducted.

Results energy decoupling rate (EDR) for Case #1 increased from 66.73% to 87.65%. As the position constraints relaxed, the mounts tended to move upwards and were widely distributed widely. EDR for Case #2 increased from 66.73% to 84.41%. In both cases, the mount stiffness decreased.

Conclusions The EDR of the cabin mounting system was significantly improved due to optimization, and the rigid body mode frequencies were optimized within the target range.

Keywords Cabin mounting system · Energy decoupling method (EDM) · Kinetic energy distribution (KED) · Mode decoupling theory · Optimization · Rubber mount

List of Symbols

x	Displacement in x direction	$\dot{\varphi}$	Acceleration in roll direction
y	Displacement in y direction	$\ddot{\theta}$	Acceleration in pitch direction
z	Displacement in z direction	$\ddot{\delta}$	Acceleration in yaw direction
\ddot{x}	Acceleration in x direction	m	Mass of cabin
\ddot{y}	Acceleration in y direction	k	Stiffness
\ddot{z}	Acceleration in z direction	$[M]$	Inertial matrix
φ	Displacement in roll direction	$[K]$	Stiffness matrix
θ	Displacement in pitch direction	$[C]$	Damping matrix
δ	Displacement in yaw direction	u	Degree of freedom
		$f_{external}$	External force
		ω	Natural frequency (rad)
		f	Natural frequency (Hz)
		\emptyset	Mode vector
		K.E	Kinetic energy
		K.E.D	Kinetic energy distribution
		EDR	Energy decoupling rate
		Objfunction	Objective function

✉ Young-Jun Park
yjpark95@snu.ac.kr

¹ Department of Biosystems Engineering, Seoul National University, 1 Gwankak-Ro, Gwankak-Gu 08826, Seoul, Republic of Korea

² Convergence Major in Global Smart Farm, Seoul National University, 1 Gwankak-Ro, Gwankak-Gu 08826, Seoul, Republic of Korea

³ Research Institute of Agricultural and Life Sciences, Seoul National University, 1 Gwankak-Ro, Gwankak-Gu 08826, Seoul, Republic of Korea

Introduction

Tractors are machines used for various agricultural tasks, such as tillage, seeding, and harvesting. Tractors are usually operated on rough surfaces, such as open fields, and require a high level of power to perform various agricultural tasks. This in turn leads to high levels of noise and vibration (Abood et al., 2015). It has been reported that tractor operators are directly exposed to this high levels of noise and vibration, which can cause various diseases. Dewangan and Patel (2023) compared the degree of hearing loss between tractor operators and non-operators and reported that the minimum audible frequency of tractor operators was higher than that of non-operators. Additionally, Koley et al. (2010) reported that tractor operators are at a high risk of developing back pain due to continuous exposure to whole body vibration. Therefore, continuous research on reducing noise and vibrations in tractors is necessary to improve the health of agricultural workers.

The tractor cabin mounting system consists of a cabin that the operator rides, and four cabin mounts that support the cabin. The cabin mounts are directly connected to the tractor body, supporting the cabin's own weight and attenuating the vibration transmitted from the body to the cabin. Rubber is primarily used as a material for cabin mounts, and its viscoelastic properties exhibits the advantage of effectively dissipating vibration energy (Anas et al., 2018). In the case of automobiles, vibrations transmitted from the road surface are mitigated through a suspension connected to the wheels, and vibrations from the engine are attenuated by using engine mounts attached separately to the engine. However, most tractors lack wheel suspension systems and engine mounts (Goering et al., 2003). Consequently, they rely solely on cabin mounts to isolate all the vibrations transmitted to the cabin. Therefore, an optimal design of the cabin mounting system is essential for reducing the noise and vibration inside the cabin.

In the design of mounting systems, setting the isolation frequency band and decoupling the rigid-body modes are of paramount importance (Adhau and Kumar, 2013). The mounting system must effectively isolate vibrations within the targeted frequency range while avoiding resonant frequencies. Therefore, the 6-DOF rigid-body mode frequencies of the cabin mounting system should be adjusted to an appropriate range based on the system characteristics. Rigid-body mode decoupling refers to the alignment of the elastic axes of an elastic support system with the inertial axes, ensuring that the rigid-body modes are completely decoupled (Park, 1994). This advantage simplifies the vibration phenomenon by preventing the excitation of one mode from inducing vibrations in other directions. Ford (1985) from Ford Motors reported improved isolation

performance within a specified frequency range by employing this methodology in the design stage of the mounting system.

Automotive OEMs have been conducting research on mounting systems since the 1960s. Engines were identified as a major source of vibration in the early stages of automobile development. Efforts have been made to isolate engine-induced vibrations by attaching rubber mounts between the engine and chassis. Timpner (1965) from General Motors proposed the theory of rigid-body mode decoupling in engine mount design. Their study argued that to realize rigid-body mode decoupling, the elastic and inertial axes of the engine mounting system should align. This alignment is essential because coupled rigid-body modes pose challenges to vibration analysis. Johnson and Subhedar (1979) from Chevrolet Motors and General Motors presented an optimization method for engine mounting system using computer simulation. In this study, for the first time, the authors introduced the energy decoupling method (EDM) to evaluate the degree of rigid-body mode decoupling using the contribution of kinetic energy. Subsequent research on engine mounting systems was conducted using the energy decoupling method to evaluate the degree of rigid-body mode decoupling and various optimization algorithms for the optimal design.

As mentioned earlier, research related to mounting systems has primarily focused on engine-mounting systems. However, no prior research has been conducted regarding the optimization of cabin-mounting systems used in vehicles such as tractors or excavators. There are limitations in directly applying optimal design techniques for engine mounting systems to cabin mounting systems. Engine mounting systems can realize complete restraint for all six DOFs by attaching engine mounts to all sides of the engine as shown in Fig. 1(a). Conversely, cabin mounting systems face significant constraints because cabin mounts must be attached only to the underside of the cabin, and the installation location of these mounts significantly influences cabin stability as depicted in Fig. 1(b). Consequently, cabin-mounting systems are considerably disadvantageous from the perspective of rigid-body mode decoupling. Additionally, owing to structural differences, separate model development is necessary for cabin mounting systems.

In this study, a 6-DOF simulation model was developed to analyze the behavior of a tractor cabin-mounting system. The developed simulation model was integrated with a genetic algorithm to optimize the design variables for the cabin mounting system, and the performance and characteristics of the optimized cabin mounting system were subsequently analyzed. The novelty and contributions of this study are as follows.

- 1) The position and stiffness of the mounts, key design variables for the tractor cabin mounting system were determined using the rigid body mode decoupling theory and energy decoupling method.

Fig. 1 Comparison of engine and cabin mounting system

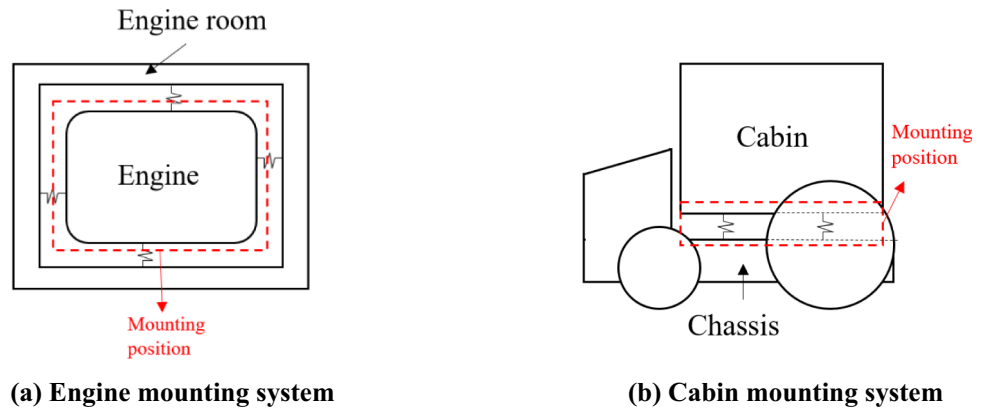


Fig. 2 Tractor used in the study

- 2) An optimization method that considers the structural and vibrational characteristics of a tractor cabin-mounting system was proposed.

Materials and Methods

Specification of Tractor

The tractor used in this study (TG300, DAE DONG Co. Ltd., Daegu, Rep.Korea) features a cabin supported by four rubber mounts, as depicted in Fig. 2. The tractor is equipped with a 104.5-kW 4-cylinder diesel engine, and the transmission consists of eight main stages capable of automatic shifting using a wet multi-plate clutch, two auxiliary stages with a continuously engaged gear, and a low-speed mode. Table 1 lists the specifications of the engine, transmission, and tires of the tractor used in the study, whereas Table 2 presents the relative positions of the four cabin mounts for the center of gravity of the cabin. As illustrated in Fig. 3, the coordinates of the cabin mounting system are defined with the cabin’s center of gravity as the origin, setting the tractor’s forward direction

Table 1 Specification of tractor used in this study

Transmission	Main part	Shift type	Wet multi-plate clutches
		Stages	8 Stages
	Sub-part	Shift type	Constant mesh
		Stages	2 Stages
Tire		Front	380/85R38
		Rear	460/85R38
Engine		Type	4-cylinder diesel
		Rated Power, kW	104.5

Table 2 Position of four mounts

	X	Y	Z
Center of gravity	0 mm	0 mm	0 mm
Front left (FL)	597 mm	382 mm	-716 mm
Front right (FR)	597 mm	-374 mm	-716 mm
Rear left (RL)	-592 mm	539 mm	-746 mm
Rear right (RR)	-592 mm	-531 mm	-746 mm

as + X, the left direction of the forward direction as + Y, and the upward direction as + Z. Table 3 lists the mass moments of inertia of the tractor cabin. Inertial properties were measured using FRF mass line method (Chen et al., 2012).

Specification of the Rubber Mount

The rubber mounts used in the study, as depicted in Fig. 4, consists of steel washers for fastening and rubber material for cushioning; the black portion in Fig. 4(b) represents the rubber material, designed with a gap. This gap is intended to create a two-stage stiffness structure that increases the rigidity when a certain load is applied, causing the upper and lower parts of the gap to come into contact. Furthermore, when viewed from the top, it is designed in a circular shape about the axis, providing uniform stiffness in all radial directions.

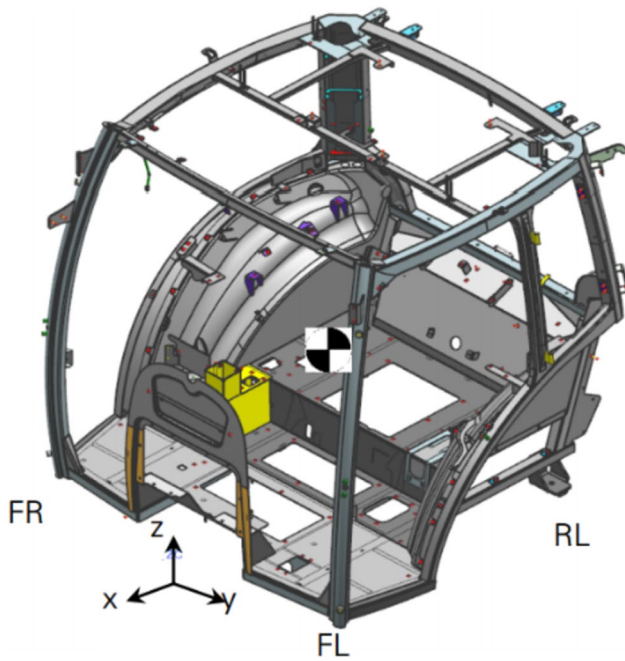


Fig. 3 Coordinate system of a cabin

Table 3 Weight and inertia of a cabin

Weight, kg	584	
I_{xx}, kgmm^2	I_{yy}, kgmm^2	I_{zz}, kgmm^2
349,118,900	15,731,737	-37,621,797
I_{yx}, kgmm^2	I_{xy}, kgmm^2	I_{yz}, kgmm^2
15,731,737	402,997,170	10,882,269
I_{zx}, kgmm^2	I_{xz}, kgmm^2	I_{zy}, kgmm^2
-37,621,797	10,882,269	397,640,170

Mathematical Formulation of 6-DOF Model

Model of a Cabin Mounting System

A 6-DOF mathematical model was formulated to predict the dynamic behavior of the cabin mounting system and conduct an eigenvalue analysis. In this study, given that the decoupling of the rigid-body modes was the primary focus, the elastic mode was not considered. Consequently, the cabin was modeled as an undeformable, rigid body. The cabin-mounting system used in this study, supported by four rubber mounts, is simplified into a model in which a rigid body is supported by four elastic springs, as shown in Fig. 5. In this representation, the mounts were modeled as translational linear springs without rotational stiffness. Various optimization studies (El Hafidi et al., 2010; Sun and Zhang, 2014) didn't consider rotational stiffness. However, this aspect is disregarded in the current study.

Equation of Motion

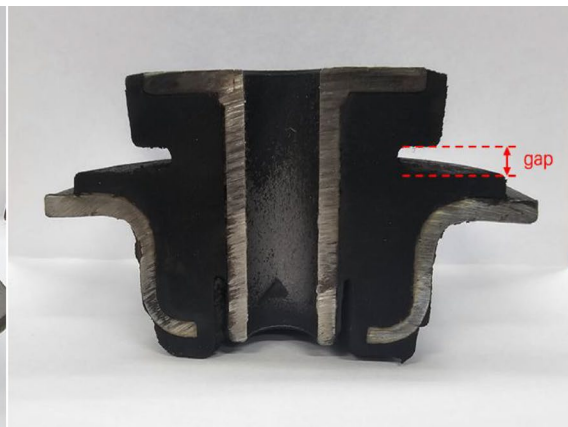
To perform eigenvalue analysis to obtain the natural frequencies and mode shapes of the rigid-body modes, the 6-DOF equations of motion for the model were derived. The equations of motion were derived by applying Newton's second law as follows: The equations for the translational motion(x, y, z) are derived as follows:

$$m\ddot{x} + k_{1x}(x - |y_1|\delta - |z_1|\theta) + k_{2x}(x + |y_2|\delta - |z_2|\theta) + k_{3x}(x + |y_3|\delta - |z_3|\theta) + k_{4x}(x - |y_4|\delta - |z_4|\theta) = 0 \tag{1}$$

$$m\ddot{x} + k_{1x}(x - |y_1|\delta - |z_1|\theta) + k_{2x}(x + |y_2|\delta - |z_2|\theta) + k_{3x}(x + |y_3|\delta - |z_3|\theta) + k_{4x}(x - |y_4|\delta - |z_4|\theta) = 0 \tag{2}$$



(a) Full view of the rubber mount



(b) Section view of the rubber mount

Fig. 4 Rubber mount used in the study

$$m\ddot{z} + k_{1z}(z - |x_1|\theta + |y_1|\varphi) + k_{2z}(z - |x_2|\theta - |y_2|\varphi) + k_{3z}(z + |x_3|\theta - |y_3|\varphi) + k_{4z}(z + |x_4|\theta + |y_4|\varphi) = 0 \tag{3}$$

The equations of motion for rotational motion (φ, θ, δ) are derived as follows.

$$I_{xx}\ddot{\varphi} + I_{yy}\ddot{\theta} + I_{zz}\ddot{\delta} + k_{1y}|z_1|(y + |x_1|\delta + |z_1|\varphi) + k_{2y}|z_2|(y + |x_2|\delta + |z_2|\varphi) + k_{3y}|z_3|(y - |x_3|\delta + |z_3|\varphi) + k_{4y}|z_4|(y - |x_4|\delta + |z_4|\varphi) + k_{1z}|y_1|(z - |x_1|\theta + |y_1|\varphi) + k_{2z}|y_2|(-z + |x_2|\theta + |y_2|\varphi) + k_{3z}|y_3|(-z - |x_3|\theta + |y_3|\varphi) + k_{4z}|y_4|(z + |x_4|\theta + |y_4|\varphi) = 0 \tag{4}$$

$$I_{yy}\ddot{\theta} + I_{xx}\ddot{\varphi} + I_{zz}\ddot{\delta} + k_{1x}|z_1|(-x + |z_1|\theta + |y_1|\delta) + k_{2x}|z_2|(-x + |z_2|\theta - |y_2|\delta) + k_{3x}|z_3|(-x + |z_3|\theta - |y_3|\delta) + k_{4x}|z_4|(-x + |z_4|\theta + |y_4|\delta) + k_{1z}|x_1|(-z + |x_1|\theta - |y_1|\varphi) + k_{2z}|x_2|(-z + |x_2|\theta + |y_2|\varphi) + k_{3z}|x_3|(z + |x_3|\theta - |y_3|\varphi) + k_{4z}|x_4|(z + |x_4|\theta + |y_4|\varphi) = 0 \tag{5}$$

$$I_{zz}\ddot{\delta} + I_{xx}\ddot{\varphi} + I_{yy}\ddot{\theta} + k_{1x}|y_1|(-x + |z_1|\theta + |y_1|\delta) + k_{2x}|y_2|(x - |z_2|\theta + |y_2|\delta) + k_{3x}|y_3|(x - |z_3|\theta + |y_3|\delta) + k_{4x}|y_4|(-x + |z_4|\theta + |y_4|\delta) + k_{1y}|x_1|(y + |z_1|\varphi + |x_1|\delta) + k_{2y}|x_2|(y + |z_2|\varphi + |x_2|\delta) + k_{3y}|x_3|(-y - |z_3|\varphi + |x_3|\delta) + k_{4y}|x_4|(-y - |z_4|\varphi + |x_4|\delta) = 0 \tag{6}$$

In the equations of motion above, the coordinates of each mount are as follows:

Mount # 1 at Front Left = (x_1, y_1, z_1) ,

Mount # 2 at Front Right = (x_2, y_2, z_2)

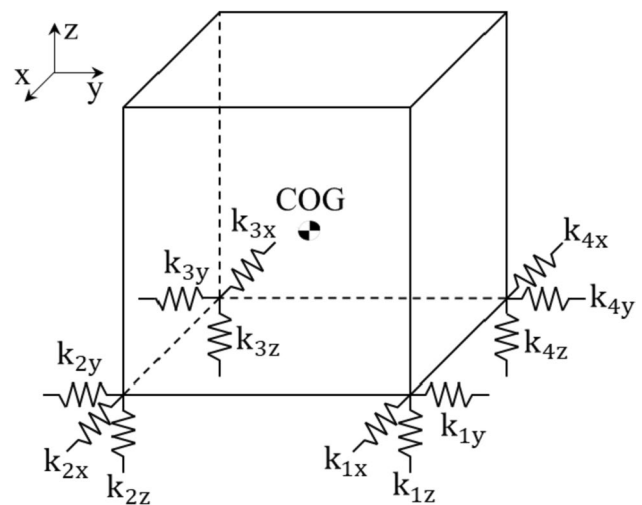


Fig. 5 Simplified model of cabin mounting system

Mount # 3 at Rear Right = (x_3, y_3, z_3) ,
Mount # 4 at Rear Left #4 = (x_4, y_4, z_4)

Eigenvalue Analysis

To obtain the natural frequencies and mode vectors for each mode of the cabin mounting system, eigenvalue analysis was conducted. Using Eqs. (1)–(6), the following coupled equation is formulated:

$$[M]\ddot{u} + [C]\dot{u} + [K]u = f_{external} \tag{7}$$

Eigenvalue analysis was conducted in a state of free vibration, where no external forces were applied. Therefore, Eq. (7) is transformed into Eq. (8):

$$[M]\ddot{u} + [K]u = 0 \tag{8}$$

In (8), u denotes the DOF vector and is expressed as follows:

$$u = [x, y, z, \varphi, \theta, \delta]^T \tag{9}$$

Performing an eigenvalue analysis on Eq. (8) allows us to obtain the system eigenvalues and eigenvectors. Eigenvalues are vectors containing information about the natural frequencies of each mode and can be represented as follows:

$$[\text{Eigenvalue}] = [\omega_1^2, \omega_2^2, \omega_3^2, \omega_4^2, \omega_5^2, \omega_6^2] \tag{10}$$

From Eq. (10), a vector containing natural frequencies in Hz units can be obtained as follows:

$$\frac{\sqrt{[\text{Eigenvalue}]}}{2\pi} = f = [f_1, f_2, f_3, f_4, f_5, f_6] \tag{11}$$

The subscript of the elements in the natural frequency vector denotes the mode order. Additionally, the eigenvector can be expressed as a (6×6) matrix containing the mode vectors for each mode as follows:

$$[\text{Eigenvector}] = [\emptyset_1, \emptyset_2, \emptyset_3, \emptyset_4, \emptyset_5, \emptyset_6] \tag{12}$$

The subscript of the elements in the eigenvector denotes the order of the mode, and each element is a (1×6) vector representing the shape in each mode.

Mode Decoupling Theory

A rigid body forms three mutually orthogonal inertial axes, with the center of mass as the origin. The inertial axes are those where no coupled forces occur when

a rigid body is rotated around an axis. For the three inertial axes, the rigid body has 6-DOF motions: three translational directions (x, y, and z) and three rotational directions (roll, pitch, and yaw). Furthermore, the elastic support system formed three elastic axes with the elastic center as the origin. The elastic axis is the axis along which, when a force is applied to the elastic support system, the direction of the force aligns with the displacement at the point of application. This axis does not induce any angular displacement in the elastic support system. The elastic axis changes according to the position, stiffness, and installation angle of the supporting elements (Kim, 1995). As shown in Fig. 6(a) and Fig. 7(a), when the stiffnesses of the two springs are identical, an elastic center is formed at the center of the beam. However, as shown in Fig. 6(b), when the stiffness is different, the elastic center is no longer at the center but shifts toward the spring with a higher stiffness. Additionally, Fig. 7 demonstrates that the elastic center changes depending on the position of the supporting spring. When the inertial axes are aligned with the elastic axes, the six rigid-body modes are completely decoupled. When the rigid-body modes are

decoupled, the vibration characteristics become simpler by preventing the excitation of one mode from inducing vibrations in other directions. This offers the advantage of an enhanced understanding of vibrations and facilitates easier control (Kim, 1995). Therefore, the decoupling of the rigid-body modes should be prioritized in mounting system designs (Angrosch et al., 2015).

The energy-decoupling method is widely used to evaluate the degree of rigid-body mode decoupling method (EDM) (Shi et al., 2020). The degree of rigid body mode decoupling is evaluated using the kinetic energy contribution of the mode vector in a specific direction. This concept is illustrated in Fig. 8.

The Total kinetic energy in the *i*-th mode of a 6-DOF vibration system can be expressed as follows:

$$K.E^i = \frac{1}{2} \omega_i^2 \sum_{k=1}^6 \sum_{j=1}^6 [M]_{kj} (\varnothing_k)_i (\varnothing_j)_i \tag{13}$$

Specifically, ω_i denotes the natural frequency of the *i*-th mode, $[M]_{kj}$ denotes the *k*, *j*-th element of the inertia matrix, and $(\varnothing_k)_i$ and $(\varnothing_j)_i$ denote the *k*, *j*-th elements of the *i*-th eigenvector; *i*, *k* and *j* = 1, 2, ..., 6

Fig. 6 Change in location of elastic center according to change in stiffness

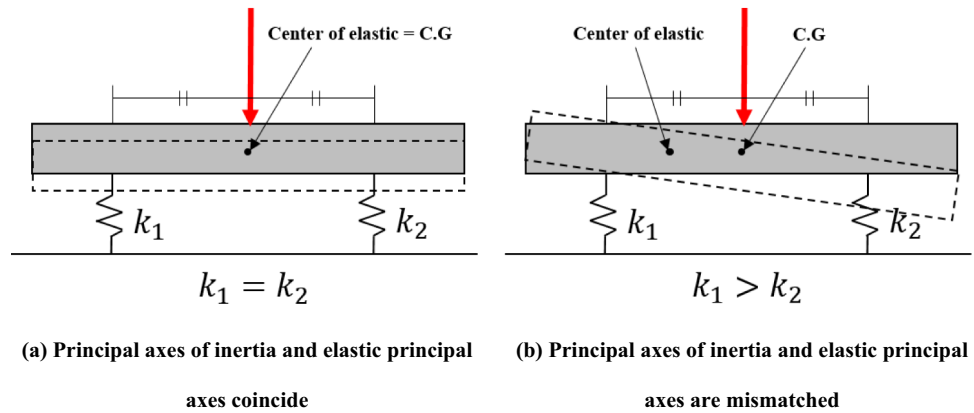
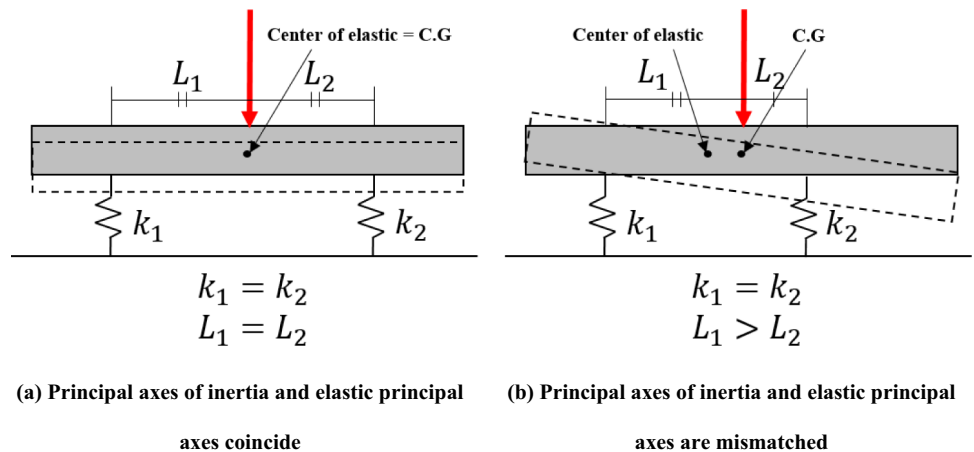


Fig. 7 Change in location of elastic center according to change in spring position



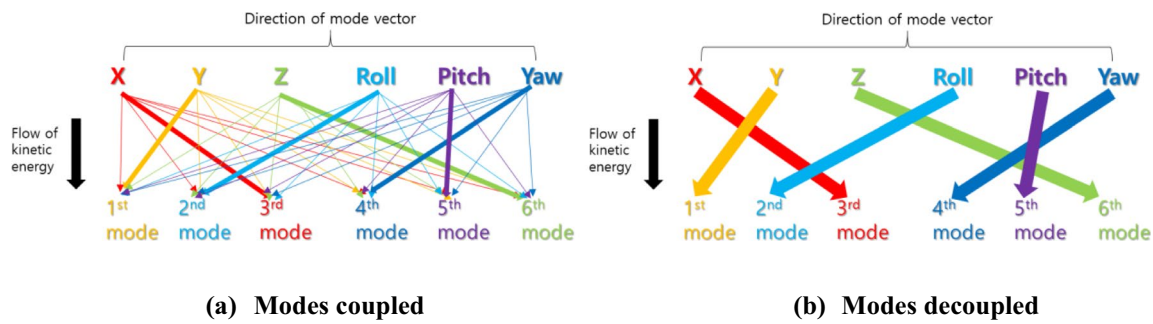


Fig. 8 Concept example of energy decoupling method (EDM)

In the generalized coordinates for the k -th DOF, the kinetic energy of the i -th mode can be expressed as follows:

$$(K.E^i)_{k^{th}generalized} = \frac{1}{2} \omega_i^2 \sum_{j=1}^6 [M]_{kj}(\varnothing_i)_k(\varnothing_i)_j \quad (14)$$

Therefore, the contribution of the mode vector to the k -th DOF mode can be expressed as the ratio of Eqs. (13) and (14). After formulation, it can be expressed as:

$$K.E.D_{ki} = \frac{\sum_{j=1}^6 [M]_{kj}(\varnothing_i)_k(\varnothing_i)_j}{\sum_{k=1}^6 \sum_{j=1}^6 [M]_{kj}(\varnothing_i)_k(\varnothing_i)_j} \quad (15)$$

Based on Eq. (15), a (6×6) kinetic energy distribution (KED) matrix can be constructed. The rows of the matrix represent the modes, and the columns represent the DOF. Therefore, the elements in the i -th row and k -th column of the matrix signify the portion of kinetic energy contributed by the mode vector of the k -th DOF in the i -th mode to the total kinetic energy of the i -th mode. The element with the highest value in each row indicates the dominant influence of the kinetic energy contribution of the mode vector in that mode. If this value is 1, then it implies that in that mode, motion occurs only in one DOF, indicating complete decoupling of that mode from other rigid-body modes.

Optimization Problem

Objective Function

In the optimization problem, the objective function is defined as a function that maximizes the factor that evaluates the degree of rigid-body mode decoupling. Furthermore, the (6×1) vector that gathers the elements with the highest values from each row of the kinetic energy distribution matrix created using Eq. (15) can be expressed as follows:

$$S = [\max(KED_{1k}), \max(KED_{2k}), \max(KED_{3k}), \max(KED_{4k}), \max(KED_{5k}), \max(KED_{6k})] \quad (16)$$

The elements of vector S represent the motion energy contribution for the mode vector corresponding to the k -th DOF with the highest contribution in each mode. This can be used as a scale to indicate the degree of rigid-body mode decoupling. Therefore, the average of the elements in vector S provides a measure of the degree of rigid-body mode decoupling in the overall system. The average of the elements in vector S is defined as the energy decoupling rate (EDR), which is employed to evaluate the degree of rigid-body mode decoupling in the system and can be expressed as follows:

$$\text{Energy decoupling rate(EDR)} = \text{Average}(S) \times 100(\%) \quad (17)$$

In the optimization problem, the objective function is defined as a function that maximizes the EDR.

$$\text{Obj function} = \text{Max(EDR)} \quad (18)$$

Optimization Variables

The optimization variables are defined as the mounting positions and stiffness values in the vertical and radial directions (k_x, k_y, k_z) of the mounts. The selected optimization variable affects the position of the elastic axis, and optimization is performed to align the elastic axis with the inertial axis.

Constraint Conditions

Natural Frequency Constraint Condition

The constraints on the natural frequencies were set to effectively isolate the main vibration components of the research

tractor and engine frequency range by shifting the resonance peak on the transmissibility curve to a lower band. A constraint was established to ensure that the natural frequency of the translational direction modes was less than 12 Hz, which is the bumping frequency of the tractor cabin mount system. Dynamic characteristic tests for the bumping frequency measurements were conducted based on the resonance method defined in ISO 10846 (Choi et al., 2018). The excitation frequency range was set to 1 Hz to 80 Hz, and it was swept with a sweep speed of 0.067 Hz/s. The imposed displacement amplitude was set to 0.254 mm (1 inch) in accordance with MIL-PRF-32407A. The static preload was set to 135 kg considering cabin's weight. Figure 9 illustrates the test used to derive the dynamic characteristics of the mounts.

Stiffness Constraint Condition

The stiffness constraints are defined based on the achievable stiffness range through shape optimization of the target mounts. Given that the mount used in this study exhibited uniform stiffness in all radial directions, both the X-direction stiffness (k_x) and Y-direction stiffness (k_y) were treated as the same single variable (k_r). The constraints in this study were

set to optimize the vertical stiffness within a range of $\pm 70\%$ of the initial stiffness and radial stiffness within $\pm 30\%$ of initial value. The initial vertical stiffness was obtained through static tests based on MIL-PRF-32407A and KS M 6005:2016 standards, whereas the radial stiffness was calculated using the values provided by the manufacturer. Given the design characteristics of the mounts, the vertical stiffness varied with the load magnitude, necessitating separate static tests. A static test for deriving the vertical stiffness was conducted by applying compressive loads in the range of 0% to 125% of the rated load, with four load cycles according to MIL-PRF-32407A, using a fatigue testing machine, as shown in Fig. 10. Displacement rate was set to 0.004 mm/s.

Position Constraint Condition

The constraints on the mounting positions must be set within an allowable range for mounting the attachment. Therefore, the initial constraints were defined to be within 20% of the initial values, ensuring that the mounting positions did not extend beyond the cabin. Additionally, to analyze the optimization patterns of the cabin mounting system, the constraints were gradually relaxed from $\pm 5\%$ to $\pm 30\%$ of the initial values. This relaxation of positional constraints allowed for the



Fig. 9 Dynamic test for the rubber mount



Fig. 10 Static stiffness test for the rubber mount

observation of changes in mount positions with respect to the extent of constraint relaxation.

Optimization Solver

The NSGA-II algorithm, a genetic algorithm, was employed to solve the optimization problem (Deb et al., 2002). Genetic algorithms are algorithms based on the principles of natural selection in a biological evolutionary process and have been widely used in mount optimization studies since the early 2000s. They iterate through the selection, crossover, and mutation rules to generate subsequent generations of the intimal design variables set until the algorithm meets the termination condition, as shown in Fig. 11. Therefore, genetic algorithms have been commonly utilized in various mount optimization studies (Sakai et al., 2001; Zheng et al., 2014; Ahn et al., 2005). The population size for each generation was set to 100, and the maximum iteration count was set to 5,000. Additionally, the termination condition was defined such that the iteration would stop if the difference between the EDR of the current generation and that of the previous generation was less than 1.0×10^{-9} . The optimization algorithm was implemented in MATLAB R2022a.

Optimization Cases

In this study, optimization was conducted for two conditions (Case #1 & Case #2). In Case #1, the stiffness and position of the mount were selected as optimization variables, and the optimization results and convergence characteristics were analyzed. In Case #2, the position of the mounts was maintained the same as the research tractor’s cabin mounting

system, while only the stiffness of the mount was selected as the optimization variable.

Results and Discussion

Static & Dynamic Test of Rubber Mount

Dynamic Test of Rubber Mount

The dynamic test results for the rubber mount are shown in Fig. 12 and listed in Table 4. The output spectrum in Fig. 12(a) shows that resonance occurs at approximately 12 Hz. Figure 12(b) confirms that the frequency range beyond 12 Hz is the isolation band after the resonance peak in the displacement transmissibility curve of the rubber mount. Therefore, optimization constraints were set to ensure that the frequency of the translational mode of the cable-mounting system was less than 12 Hz.

Static Stiffness

The static test results for the rubber mounts are shown in Fig. 13 and listed in Table 5. In Fig. 13, it can be observed that the slope of the curve changes when a certain load is applied. This is because the mount-shaped design was intended to exhibit an increase in stiffness with increasing load. For the research tractor, considering that the mount stiffness was within the range of the secondary stiffness curve with the cabin’s own weight alone, the secondary stiffness was set as the initial design parameter. Rubber mounts exhibit hysteresis owing to the viscoelastic behavior

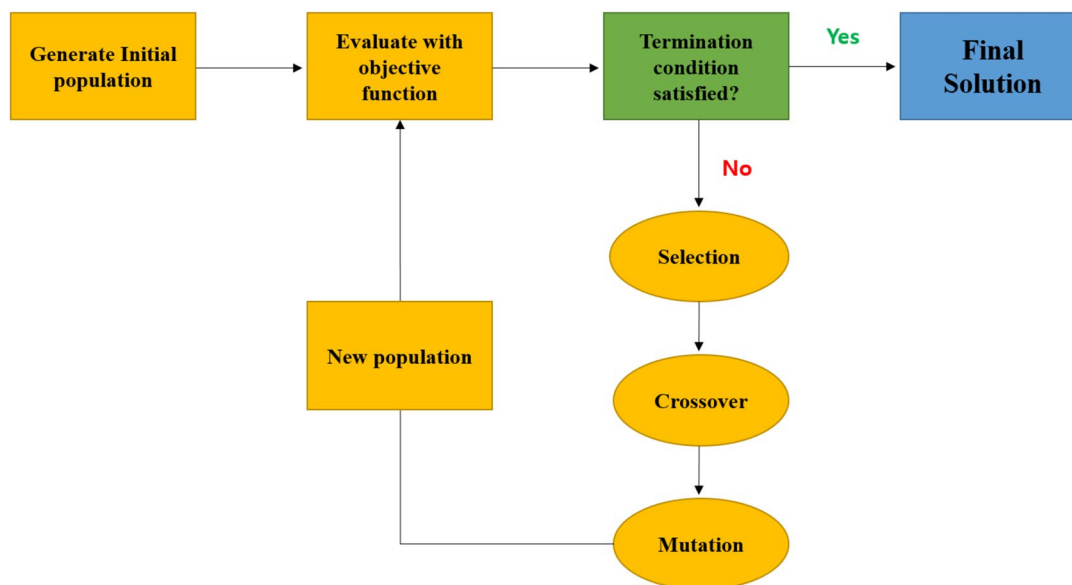
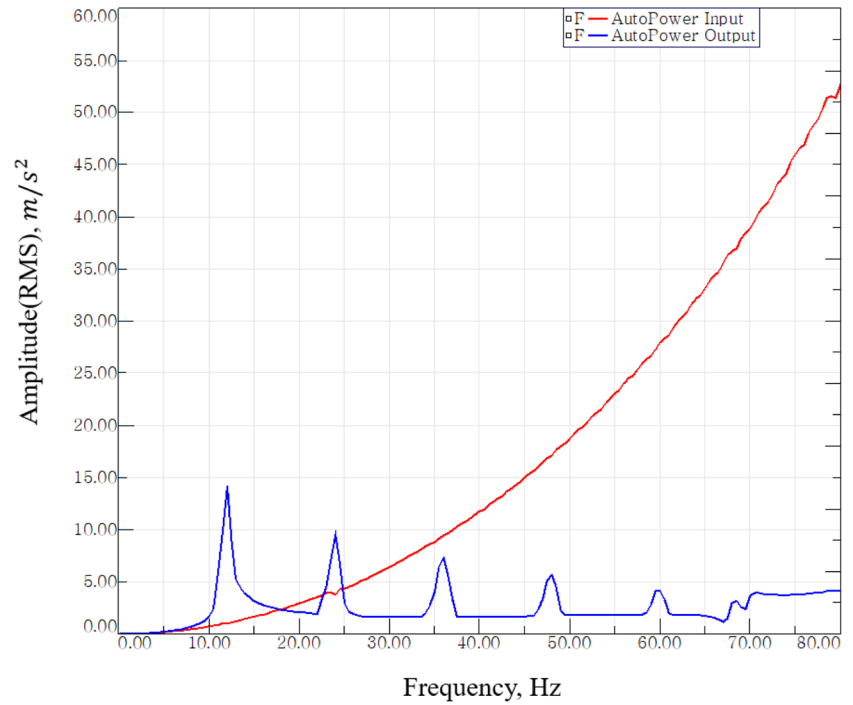
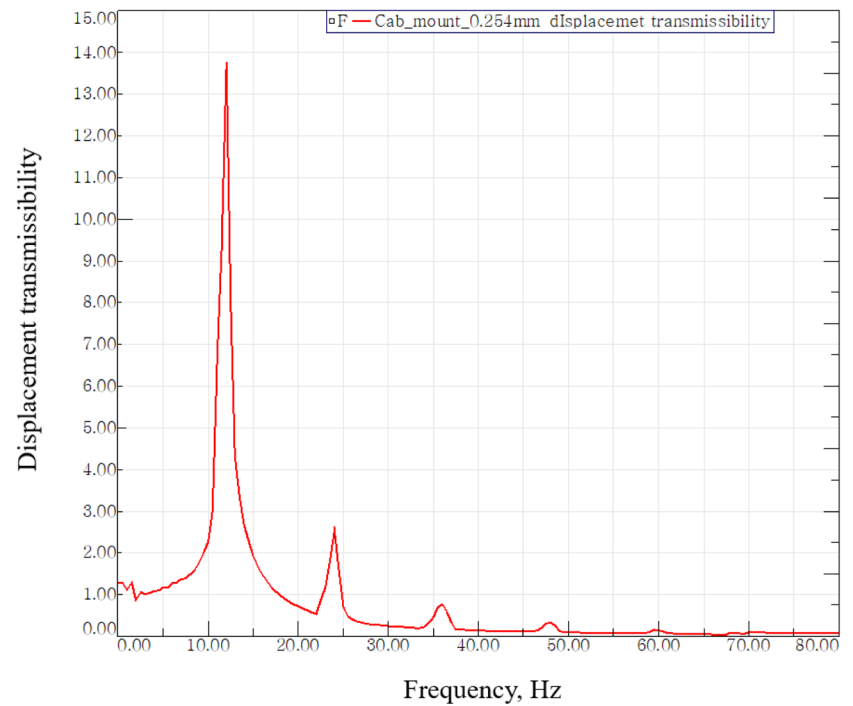


Fig. 11 Optimization process using genetic algorithm

Fig. 12 Results of dynamic test for the rubber mount



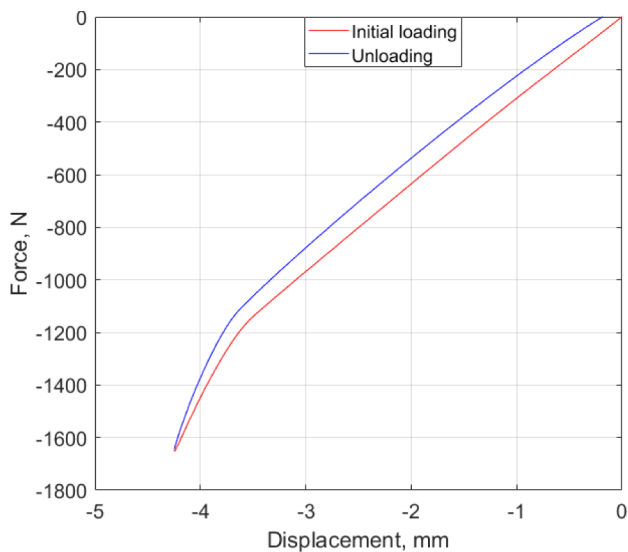
(a) Input and output spectrum for rubber mount



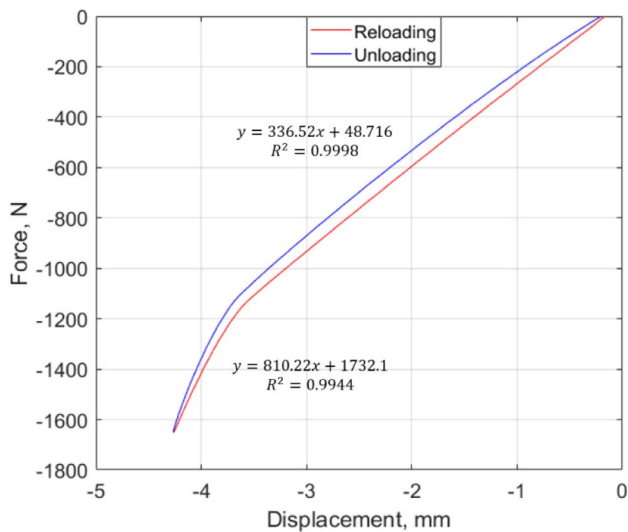
(b) Displacement transmissibility for rubber mount

Table 4 Dynamic characteristics for rubber mount

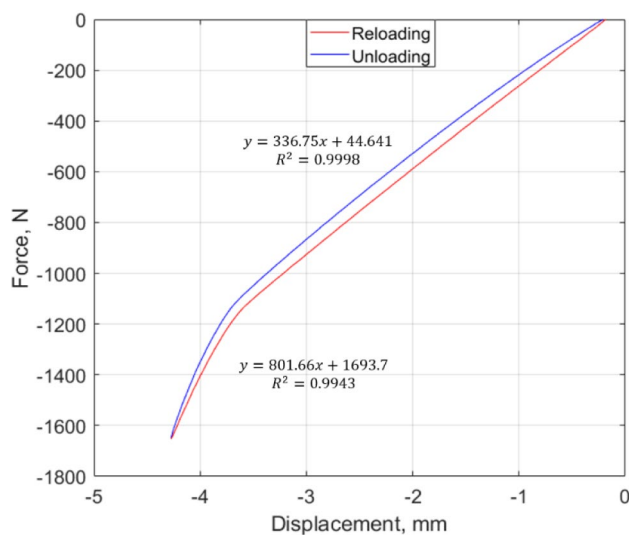
Natural frequency, Hz	Displacement transmissibility	Dynamic stiffness, N/mm	Damping Coefficient	Damping ratio
12	13.79	767.46	0.1178	0.0364



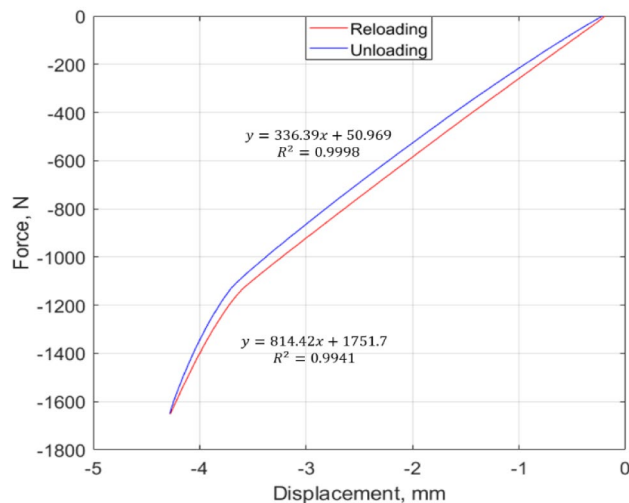
(a) Initial loading and unloading



(b) 1st cycle



(c) 2nd cycle



(d) 3rd cycle

Fig. 13 (continued)

Table 5 Results of static stiffness along Z-direction

Cycle	Stiffness of 1st slope, N/mm	Stiffness of 2nd slope, N/mm
1st	336.75	801.66
2nd	336.52	810.22
3rd	336.39	814.42

Fig. 13 Force–displacement curve from static stiffness test for rubber mount

Table 6 Results of optimization for Case #1

Variable	Before	After
Vertical stiffness of mount, N/mm	810.000	482.010
Radial stiffness of mount, N/mm	470.820	142.130
Position of mount #1, mm	(597, 832, -716)	(651, 402, -644)
Position of mount #2, mm	(597, -832, -716)	(651, -402, -644)
Position of mount #3, mm	(-592, -539, -746)	(-554, -553, -691)
Position of mount #4, mm	(-592, 539, -746)	(-554, 553, -691)
EDR, %	66.73	87.65

of the material, resulting in different unloading and reloading curves. The static stiffness was derived based on the reloading curve, considering that the rubber mount always supported the weight of the cabin.

Optimization

Case #1 (Optimization Variable: Stiffness & Position for Rubber Mount)

In Case #1, the optimization results for the mount stiffness lead to an improvement in the EDR from 66.73% to

Table 7 Natural frequency and kinetic energy distribution rate (KEDR) before optimization for Case #1

DOF		X	Y	Z	RX (roll)	RY (pitch)	RZ (yaw)
Natural frequency, Hz		5.15	4.32	10.45	13.36	12.96	8.26
KEDR	X	67.66	0.07	0.00	13.81	18.05	0.08
	Y	0.16	64.03	0.01	17.09	17.70	0.70
	Z	0.00	0.00	99.99	0.01	0.00	0.00
	RX(roll)	0.06	35.85	0.00	35.00	29.33	0.00
	RY(pitch)	32.10	0.04	0.00	32.77	34.50	0.01
	RZ(yaw)	0.02	0.01	0.00	1.32	0.42	99.22

Table 8 Natural frequency and kinetic energy distribution rate (KEDR) after optimization for Case #1

DOF		X	Y	Z	RX (roll)	RY (pitch)	RZ (yaw)
Natural frequency, Hz		3.92	3.44	8.67	7.86	8.66	4.88
KEDR	X	88.33	0.03	0.00	0.65	10.67	0.08
	Y	0.06	79.06	0.00	19.62	0.64	0.65
	Z	0.00	0.00	100.00	0.00	0.00	0.00
	RX(roll)	0.01	20.85	0.00	75.38	4.35	0.00
	RY(pitch)	11.57	0.01	0.00	2.87	83.91	0.00
	RZ(yaw)	0.03	0.05	0.00	1.48	0.42	99.27

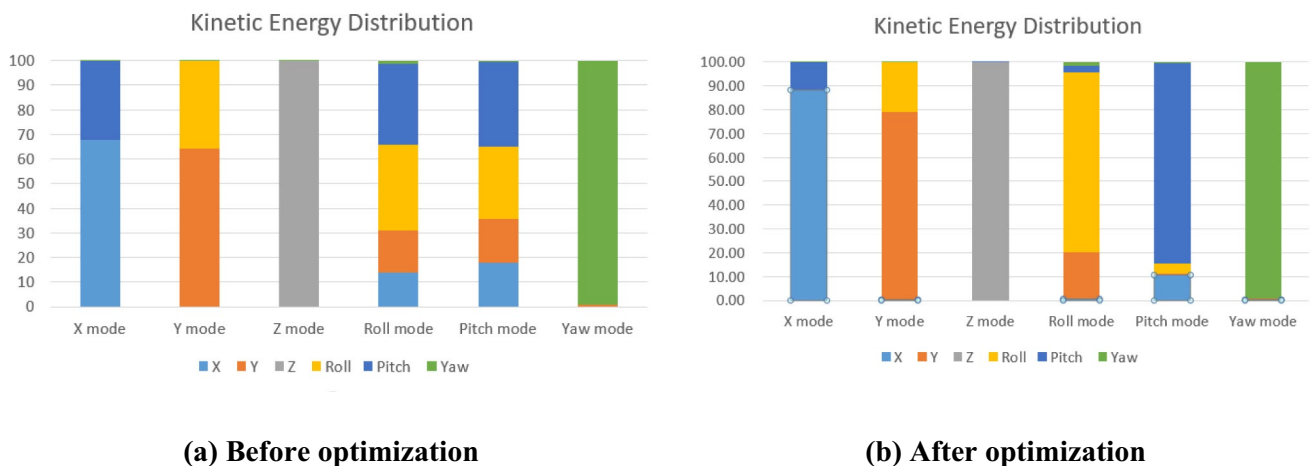
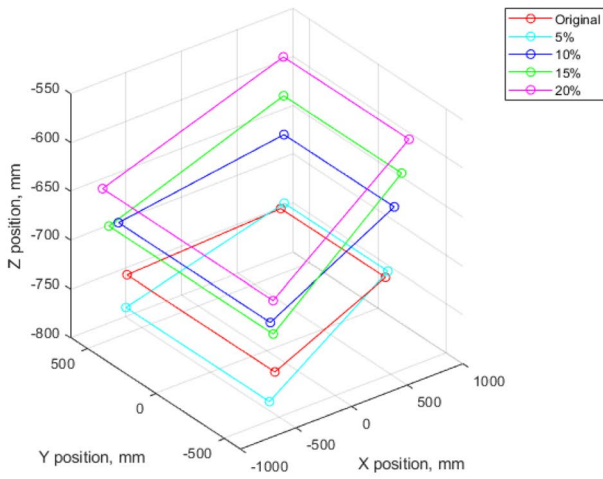
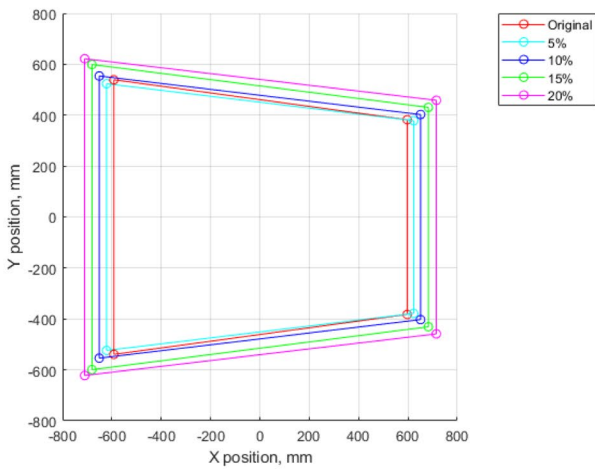


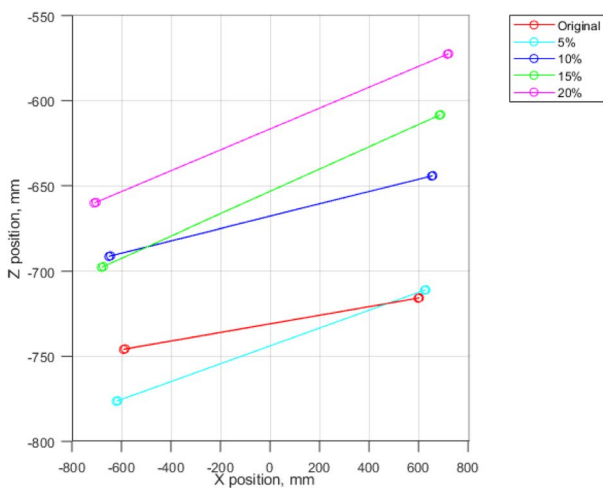
Fig. 14 Visualization of kinetic energy distribution rate for Case #1



(a) 3D view for position of mounts

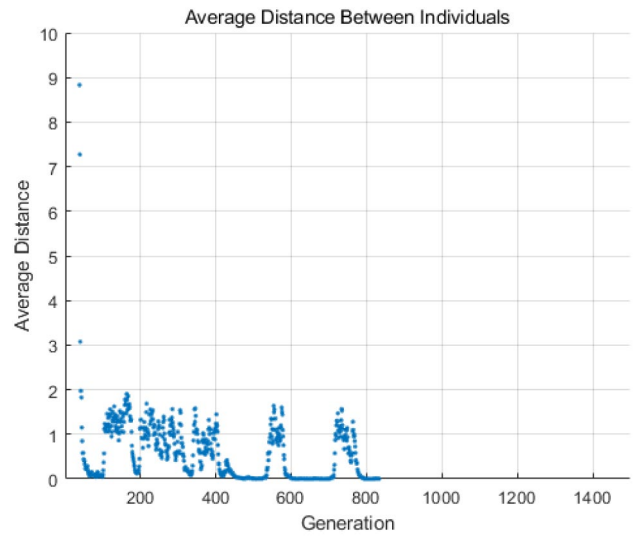


(b) View of X–Y plane for position of mounts

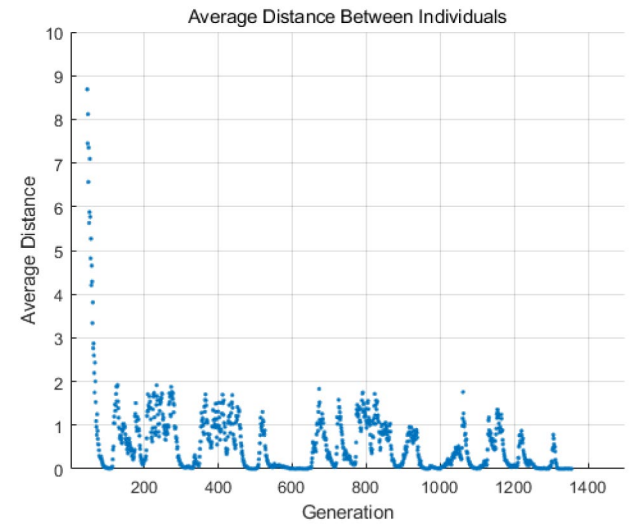


(c) View of X–Z plane for position of mounts

Fig. 15 Change in position of mounts according to change in position constraint condition for Case #1



(a) Constraint for position: $\pm 5\%$

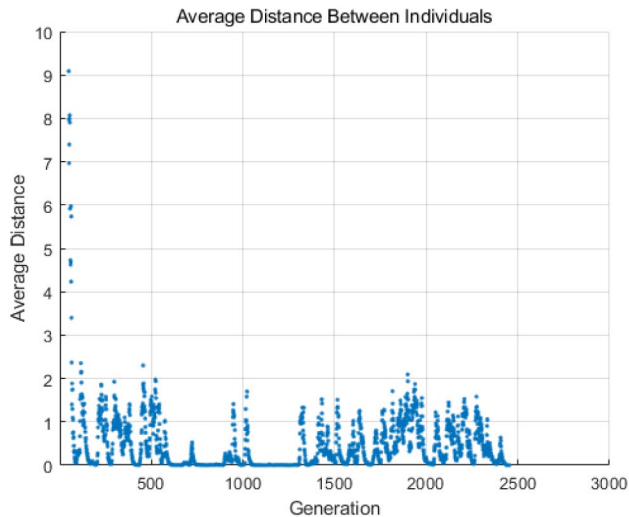


(b) Constraint for position: $\pm 10\%$

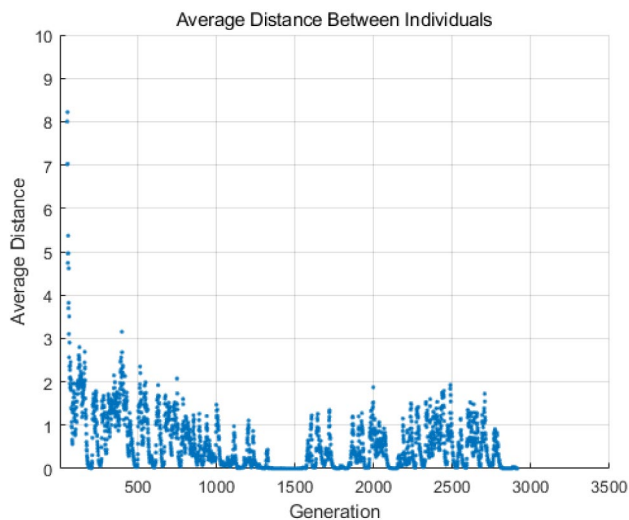
Fig. 16 Population diversity of optimization algorithm according to the change in constraint condition for Case #1

87.65%, as presented in Table 6. Furthermore, Tables 7 and 8 present the natural frequencies and kinetic energy distribution rates for each mode before and after optimization, respectively. The degree of rigid-body mode decoupling significantly improved for all modes, with the exception of Z and Yaw modes. Figure 14 shows the distribution of kinetic energy before and after optimization, providing a visual confirmation of the simplification of motion in the roll and pitch modes.

In Case #1, the optimization results for the mount position, as shown in Fig. 15(a), indicate an upward shift in the



(c) Constraint for position: $\pm 15\%$



(d) Constraint for position: $\pm 20\%$

Fig. 16 (continued)

mount position. Consequently, X- and Y-direction elastic

Table 9 Results of optimization for Case #2

Variable	Before	After
Vertical stiffness of mount, N/mm	810.000	490.000
Radial stiffness of mount, N/mm	470.820	141.250
EDR, %	66.73	84.41

axes also shift upward. This is attributed to the improvement in the degree of rigid-body mode decoupling owing to the closer proximity of the elastic axis to the inertial axis. Figure 15(a) demonstrates that as the constraint on the position are relaxed from $\pm 5\%$ to $\pm 20\%$, the mount's position shifted upward. This signifies that the optimization process results in an upward movement of the elastic axis, reducing the distance from the inertial axis. Moreover, the decrease in the mount stiffness is presumed to influence the movement of the elastic axis. Figure 15(b) illustrates the tendency of the mount to distribute widely with the relaxation of the position constraints, confirming that the optimization is conducted in a manner that does not compromise the stability of the cabin.

Figure 16 illustrates the average distance between the components of the current and previous generations when NSGA-II is applied. This shows the convergence characteristics with respect to the relaxation of the constraints on the mount position. As the constraints on the position of the mount were relaxed, the number of iterations increased, indicating an expansion of the objective function space owing to the relaxation of the constraint.

Case #2 (Optimization Variable: Stiffness for Rubber Mount)

In Case #2, given the optimization of the mount stiffness, the EDR increases from 66.73% to 84.41%, as shown in Table 9. The smaller improvement in the EDR when compared to Case #1 is attributed to the remaining fixed position of the mount. The stiffness in both the vertical and radial directions decreased, similar to Case #1. Table 10 lists the optimized natural frequencies and kinetic energy distribution rates for each mode under the conditions of Case #2. The lower improvement in the EDR for roll and pitch modes when compared to Case #1 is attributed to the inability to realize an upward movement of the elastic axis through the upward movement of the mounts. Figure 17 visually depicts the distribution of kinetic energy before and after optimization, highlighting the simplification of motion in the roll and pitch modes. Figure 18 illustrates the convergence characteristics of the optimization for Case #2. This shows a decrease in the number of iterations when compared to Case #1, indicating a reduction in the objective function space owing to the decrease in the number of optimization variables.

Conclusion

In this study, a 6-DOF simulation model was developed to analyze the behavior of a tractor cabin-mounting system. To avoid resonance frequencies and enhance the degree of rigid body mode decoupling, the design variables of the cabin mounting system were optimized using the NSGA-II, one

Table 10 Natural frequency and kinetic energy distribution rate (KEDR) after optimization for Case #2

DOF		X	Y	Z	RX (roll)	RY (pitch)	RZ (yaw)
Natural frequency, Hz		3.68	3.24	8.75	7.99	8.49	4.52
KEDR	X	85.01	0.05	0.06	1.86	12.51	0.16
	Y	0.08	78.26	0.03	19.29	1.85	0.74
	Z	0.00	0.00	99.30	0.05	0.59	0.00
	RX(roll)	0.01	21.58	0.20	69.84	9.56	0.00
	RY(pitch)	14.81	0.02	0.40	7.76	74.97	0.01
	RZ(yaw)	0.10	0.09	0.01	1.20	0.53	99.09

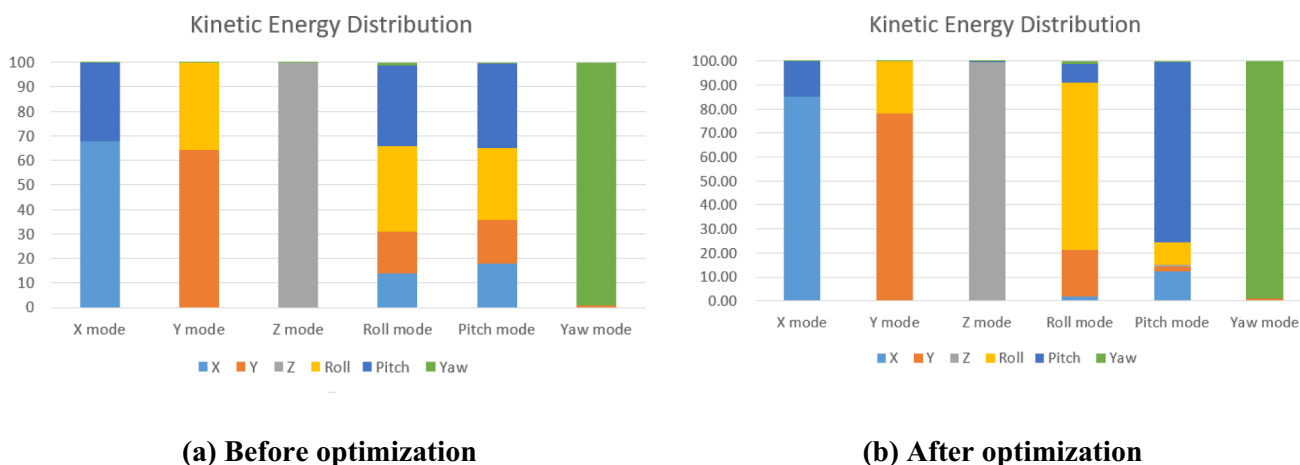


Fig. 17 Visualization of kinetic energy distribution rate for Case #2

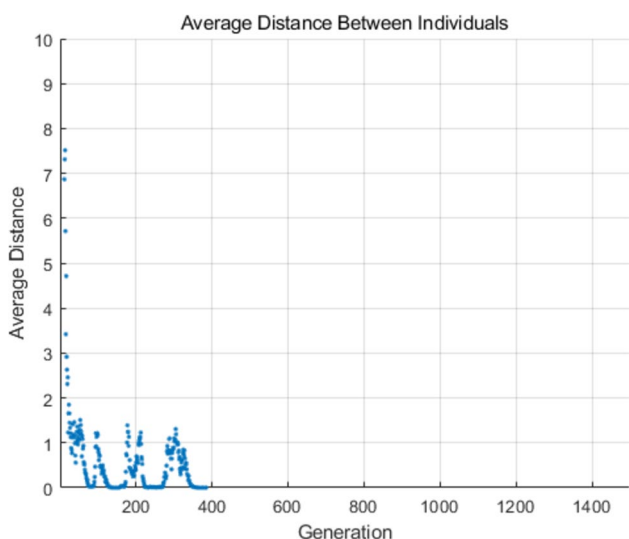


Fig. 18 Population diversity of optimization algorithm according to the change in constraint condition for Case #2

of the genetic algorithm. The conclusions of this study are as follows.

1. In Case #1, in which the stiffness and position of the mounts were selected as the optimization variables, the EDR of the cabin mounting system improved from 66.73% to 87.65%. The decrease in mount stiffness and upward movement of the mount position contributed to the elastic axis approaching the inertial axis, leading to an increase in the EDR. Additionally, the motions of the roll and pitch modes were simplified. The convergence characteristics of the optimization showed that as the constraints on the position of the mount were relaxed, the number of iterations until convergence increased.
2. In Case #2, in which only the stiffness of the mount was selected as the optimization variable, the EDR improved from 66.73% to 84.41%. The lower improvement rate in the EDR when compared to Case #1 is attributed to the constraint on the movement of the mount position, preventing the upward movement of the elastic axis. This restriction resulted in relatively low optimization of the

degree of decoupling of the roll and pitch modes. The convergence characteristics of the optimization showed a decrease in the number of iterations when compared to Case #1, which was attributed to the reduction in the optimization variables, and thereby, affecting the objective function space.

- It was established that that positioning the mount closer to the center of gravity of the cabin is effective from the perspective of rigid-body mode decoupling. Furthermore, by observing the tendency of the cabin mount to spread widely with the relaxation of position constraints, it was confirmed that the optimization was performed in a direction that did not compromise cabin stability.

In conclusion, the optimization of the cabin mounting system resulted in a significant improvement in the degree of rigid-body mode decoupling. Additionally, the natural frequencies of the rigid-body mode in the translational direction were within the target range.

Acknowledgements This work was supported by Korea Institute of Planning and Evaluation for Technology in Food, Agriculture and Forestry(IPET) through Eco-friendly Power Source Application Agricultural Machinery Technology Development Program, funded by Ministry of Agriculture, Food and Rural Affairs(MAFRA)(322047-5).

Funding Open Access funding enabled and organized by Seoul National University.

Data Availability The datasets used and/or analysed during the current study available from the corresponding author on reasonable request.

Declarations

The authors have no conflicting financial or other interests.

Open Access This article is licensed under a Creative Commons Attribution 4.0 International License, which permits use, sharing, adaptation, distribution and reproduction in any medium or format, as long as you give appropriate credit to the original author(s) and the source, provide a link to the Creative Commons licence, and indicate if changes were made. The images or other third party material in this article are included in the article's Creative Commons licence, unless indicated otherwise in a credit line to the material. If material is not included in the article's Creative Commons licence and your intended use is not permitted by statutory regulation or exceeds the permitted use, you will need to obtain permission directly from the copyright holder. To view a copy of this licence, visit <http://creativecommons.org/licenses/by/4.0/>.

References

- Abood, A. M., Moses, S. C., & Lawrence, A. K. A. (2015). Evaluation of Tractor Noise Level during Tillage Operation with a Disc Plough. *European Academic Research*, 3(5410), 5421.
- Adhau, A., & Kumar, P. V. (2013). Engine mounts and its design considerations. *International Journal of Engineering Research & Technology*, 2(11), 2278–181.
- Ahn, Y. K., Kim, Y. C., Yang, B. S., Ahmadian, M., Ahn, K. K., & Morishita, S. (2005). Optimal design of an engine mount using an enhanced genetic algorithm with simplex method. *Vehicle System Dynamics*, 43(1), 57–81.
- Anas, K., David, S., Babu, R. R., Selvakumar, M., & Chattopadhyay, S. (2018). Energy dissipation characteristics of crosslinks in natural rubber: An assessment using low and high-frequency analyzer. *Journal of Polymer Engineering*, 38(8), 723–729.
- Angrosch, B., Plöchl, M., & Reinalter, W. (2015). Mode decoupling concepts of an engine mount system for practical application. *Proceedings of the Institution of Mechanical Engineers, Part k: Journal of Multi-Body Dynamics*, 229(4), 331–343.
- Chen, J., Randall, R. B., Peeters, B., Van Der Auweraer, H., & Desmet, W. (2012). Inertial property estimation by the modal model method. *International Conference on Noise and Vibration Engineering*, 17–19.
- Choi, K., Oh, J., Ahn, D., Park, Y. J., Park, S. U., & Kim, H. S. (2018). Experimental study of the dynamic characteristics of rubber mounts for agricultural tractor cabin. *Journal of Biosystems Engineering*, 43(4), 255–262.
- Deb, K., Pratap, A., Agarwal, S., & Meyarivan, T. A. M. T. (2002). A fast and elitist multiobjective genetic algorithm: NSGA-II. *IEEE Transactions on Evolutionary Computation*, 6(2), 182–197.
- Dewangan, K. N., & Patel, T. (2023). Noise exposure and hearing loss among tractor drivers in India. *Work*, 74(1), 167–181.
- El Hafidi, A., Martin, B., Loreda, A., & Jeco, E. (2010). Vibration reduction on city buses: Determination of optimal position of engine mounts. *Mechanical Systems and Signal Processing*, 24(7), 2198–2209.
- Ford, D. M. (1985). An analysis and application of a decoupled engine mount system for idle isolation (No. 850976). *SAE Technical Paper*
- Goering, C. E., Stone, M. L., Smith, D. W., & Turnquist, P. K. (2003). Off-road vehicle engineering principles (pp. 383–462). St. Joseph, Mich.: American Society of Agricultural Engineers
- Johnson, S. R., & Subhedar, J. W. (1979). Computer optimization of engine mounting systems. *SAE Technical Paper*, 790974, 19–26.
- Kim, U. G. (1995). A Study on the Elastic Mounting System for Marine Engine (I). *Journal of Korea Fishing Vessel Association*, 64, 25–29.
- Koley, S., Sharma, L., & Kaur, S. (2010). Effects of occupational exposure to whole-body vibration in tractor drivers with low back pain in Punjab. *The Anthropologist*, 12(3), 183–187.
- Park. (1994). The Design of Vibration Isolation for Ultra-Precision Machine. *Korean Society for Precision Engineering*, 171–176.
- Sakai, T., Iwahara, M., Shirai, Y., & Hagiwara, I. (2001). Optimum engine mounting layout by genetic algorithm. *SAE Transactions*, 110(2), 496–502.
- Shi, H., Shi, W., Yang, C., Liu, G., Fan, Z., & Chen, Z. (2020). Rubber Stiffness Optimization for Floor Vibration Attenuation of a Light Bus Based on Matrix Inversion TPA. *Shock and Vibration*, 2020, 1–14.
- Sun, X., & Zhang, J. (2014). Performance of earth-moving machinery cab with hydraulic mounts in low frequency. *Journal of Vibration and Control*, 20(5), 724–735.
- Zheng, L., Duan, X., Deng, Z., & Li, Y. (2014). Multi-objective optimal design of magnetorheological engine mount based on an improved non-dominated sorting genetic algorithm. *In Active and Passive Smart Structures and Integrated Systems*, 9057, 839–848